Metallurgical evaluation of laser additive manufactured Ti6Al4V components

Kalenda Mutombo

MSM/Light Metals, Council for Scientific and Industrial Research (CSIR), South Africa
KMutombo@csir.co.za

Abstract

Ti6Al4V laser manufactured samples were analysed using optical and scanning electron microscopy equipped with X-ray micro-analyser. The presence of α, α_2, β, α′, and α″ phases were determined using differential scanning calorimetry. The angle of contact between single deposited layer and Ti6Al4V base as well as the tensile properties of the component were evaluated. Powdered metal globularization, size segregation, un-melted or semi-melted particles and chemical surface contamination were revealed. Very few globules were in perfect contact with the Ti6Al4V base. The lack of wettability, between the Ti6Al4V base and molten Ti6Al4V powder, and the partial immiscibility evidently is the result of relatively higher interfacial energy between the solid and liquid compared to the surrounding atmosphere-liquid and solid-gas interfacial energies. The produced surface finish was relatively rougher. A mixture of columnar grains, layer bands and fully martensitic structure was developed during the laser additive manufacturing due to fast cooling and heat input localization. Ultimate and yielding strength were relatively higher in the as manufactured and polished parts, however lower tensile properties were revealed mil-annealed.

Keywords: laser additive manufacturing, microstructure, tensile properties, Ti6Al4V alloy

1. Introduction

The laser additive manufacturing (LAM) process, which uses a high energy fibre laser to fuse powdered metal, presents some advantages over conventional manufacturing processes such as combining manufacturing and post-treatment process, saving time and lower manufacturing costs on low-volume components. However components fabricated following this route contain some metallurgical defects. Surface roughness, internal and external pores, residual stresses and uncontrollable microstructure are the draw-backs. Consequently the associated mechanical properties and the performance of the produced component for a specific application may be compromised. Numbers of additive manufacturing processes of metallic components are available nowadays. They melt or soften metal powder to create component through a sequential layering. Electron Beam Melting (EBM), Electron Beam Freeform Fabrication (EBF), Selective Laser Melting (SLM), Laser Engineered Net Shaping (LENS), Direct Metal Laser Sintering (DMLS) and Selective Laser Sintering (SLM) are the mostly used techniques.

The microstructure of the LAM components has been strongly characterized. A mixture of columnar grains, layer bands and martensitic structure is the typical microstructure of LAM parts [1, 3-5, 11, 14]. The presence and effect of flaws, such as surface roughness, porosity and layer bands, on tensile and fatigue properties have been investigated [1, 4-6, 11]. However, the correlation microstructure/process parameters such as laser power, spot size and scanning speed still need to be deeply understood [2, 3, 6, 7, 9, 12, 13, 15, 16]. So far, manufacturing components using LAM process requires some modifications and accurate processing variables. Therefore, this investigation is evaluating the metallurgical aspects of laser additive manufactured Ti6Al4V components obtained through different methods such as laser engineered net shaped and direct metal laser sintering.

2. Experiment and Materials

Ti6Al4V component were manufactured using LENS or DMLS laser techniques. A single layer of Ti6Al4V powder alloy was as well deposited on Ti6Al4V base of 6 mm thick using LENS process. LENS and DMLS components and single layer were analysed using optical and scanning electron microscopy equipped with X-ray micro-analyser. The sample was previously ultrasonically cleansed in ethanol and superficially cold mounted for powder metal-base retention. The cross-section was hot mounted and subsequently polished and etched using the conventional metallographic preparation procedure. The surface roughness measurement was made using optical method and image analysis.
Ti6Al4V dog-borne sample produced by DMLS powder bed method was used for tensile testing. The sample gauge length, breath and width were 23.50, 3.99 and 4.01 mm, respectively. Tensile properties and fracture analysis of the as received and heat treated samples were respectively studied using INSTRON™ Servo Hydraulic testing machine, and scanning electron microscope. The heat treatment of the dog-borne shape samples was performed using the Zerion™ vertical vacuum furnace.

3. Results and discussion

3.1. Microstructural analysis

3.1.1. First deposited layer

The as deposited single layer of Ti6A4V alloy and un-melted or semi-melted particles are respectively shown in Figures 1a and 1b. Powdered metal globularization, size segregation and un-melted or semi-melted finer particles are revealed. Black and white areas on the deposited globules are also evident.
The SEM analysis of the polished and etched cross-section of the single layer-base is shown in Figure 2. Most Ti6Al4V globules, as seen in Figure 1, are not directly in contact with the Ti6Al4V base. The occurrence of globule formation is the evidence of low wettability i.e. the strength of the solid/liquid interaction between the base and the deposited liquid metal is weak compared to that of liquid/liquid interaction. Since the average angle of contact was in between 90^{o} and 180^{o}, see Figure 2a.
X-ray microanalysis of the polished and etched cross-section of the single layer-base is shown in Figure 3. The interface is filled with some contaminating layer and very fine un-melted alloy powder. Very few globules are in perfect contact with the base.

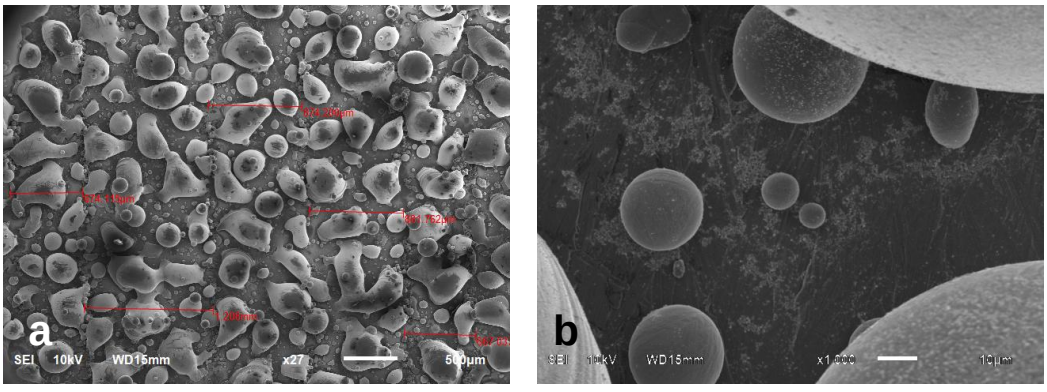

Figure 1. SEM micrographs of the as-deposited single layer showing, a) the globularization, size segregation, and b) un-melted or semi-melted particles of Ti6Al4V powder

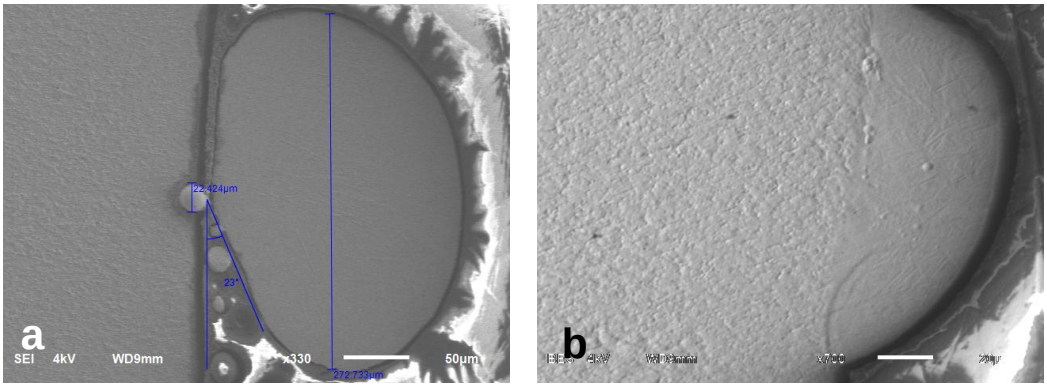

Figure 2. SEM cross-section of the as-deposited single layer/base, revealing the base-powdered Ti6Al4V interface layer or interface bonding and the base –liquid metal contact angle

According to the Young's equation, the perfect wetability between the base and molten Ti6Al4V powder will be given by an angle of contact equals to zero. And the total immiscibility by angle equals to 180^{o}. Therefore the interfacial energy between the solid and the surrounding atmosphere should be relatively higher compared to liquid-gas and solid-liquid interfacial energies.

$$\cos\theta c = (SG - SL) / LG$$

Where, SG, SL, LG and θc are respectively interfacial energy between solid-gas, solid-liquid metal, liquid metal-gas and angle of contact between.

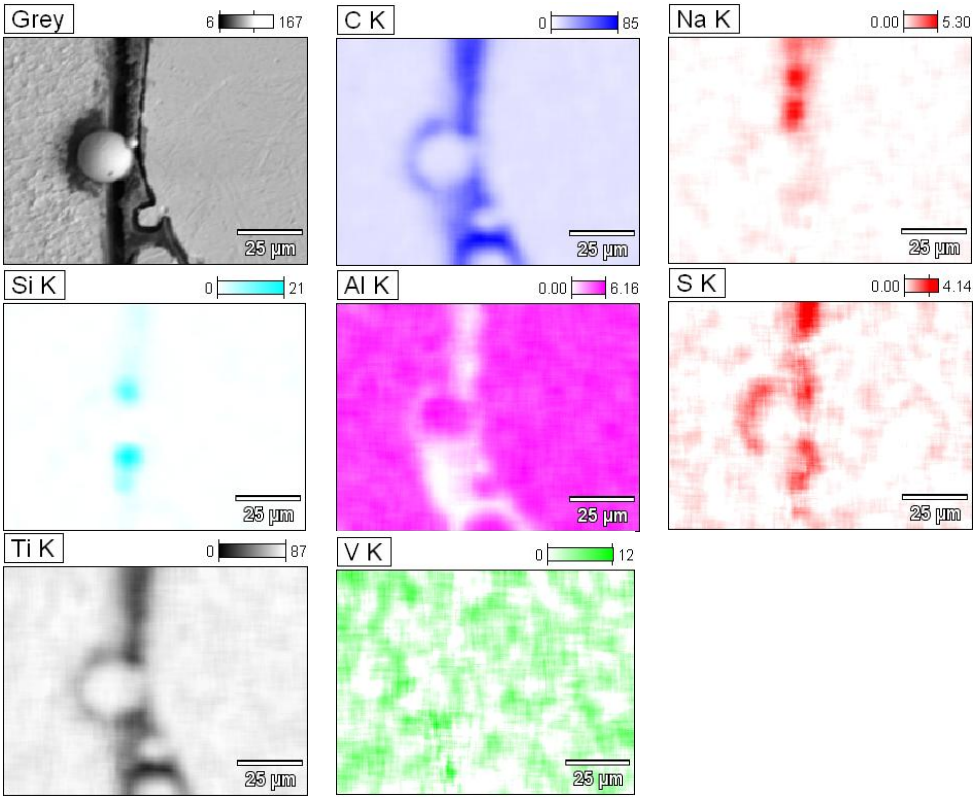

Figure 3. X-ray microanalysis of the single layer-base Ti64 alloy, revealing the presence of contaminating elements such as C, Na, Si, and S.

The laser power could be enough to melt the Ti6Al4V powders; however the base surface and/or the powder chemically contaminated by carbon, sodium, silicon and sulphur led to

lower interfacial energy between the base, deposited liquid metal and the surrounding atmosphere, which resulted in lack of wettability.

3.1.2. Surface roughness

The surface finish of the as manufactured and heat treated Ti6Al4V LAM component is respectively shown in Figures 3 and 4. Surface roughness of LAM produced part is dependent on operating conditions and characteristics of powder used. Larger powder particles have been found to increase the energy of the molten pool. This results in rough surface finish of the component whereas smaller particles create a stable molten pool and smooth part surface finish [8]. The morphology and size of the powder particles influences the flowability. Very small particles show low flowability due to clogging of the nozzles as these powders coagulate thereby restricting the flow. However, intermediate powder particle size gives the highest flowability through the nozzles [13]. Spherical powder morphologies are more preferable during laser melting due to its high flowability as well as layer stacking and melting uniformity [12]. Smaller sized powder particles are easier to melt (i.e. lower laser power is needed) compared to larger particles due to the less surface area of the former. On the other hand, powder characteristics such as surface tension, cohesive bonds, wall friction, as well as electrostatic force determine powder flowability [12, 16]. Reducing the specific energy (Es) (E_s=P (laser power) x S (scanning velocity)/ ∅(laser spot)) and increasing the deposition rate while maintaining the correct morphology and powder particle size result in a smooth surface, however using high specific energy and low deposition rate produce an increase in surface roughness. And, the surface becomes rougher when too much remelting of the previous layers occurs as a result of increasing E_s and lowering the deposition rate [13].

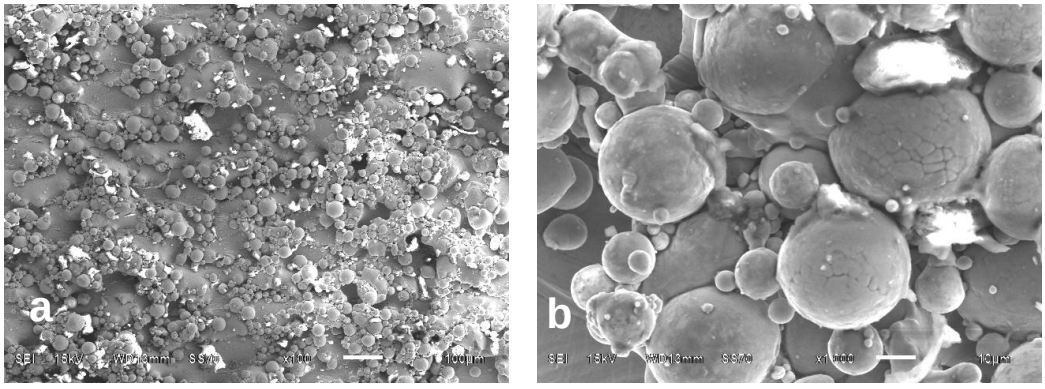

Figure 3. Typical surface finish of the as manufactured Ti6Al4V LAM component revealing un-melted powder particles and chemical contamination

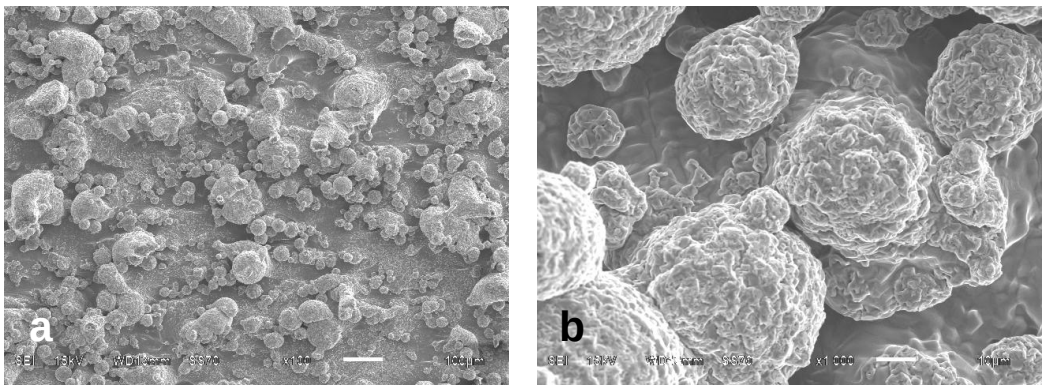

Figure 4. Typical surface finish of the heat treated Ti6Al4V LAM component revealing a surface free of un-melted powder particles and chemical contamination

The roughness profile of the as manufactured heat treated LAM component and is shown in Figures 5 and 6. The as manufactured component appeared to be rougher than the heat treated finish surface. The maximum height (Rt) of the profile for both as manufactured and heat treated is shown in Figure 6. The as manufactured component showed higher amplitude value (red top graph) than the heat treated LAM component (blue bottom graph).

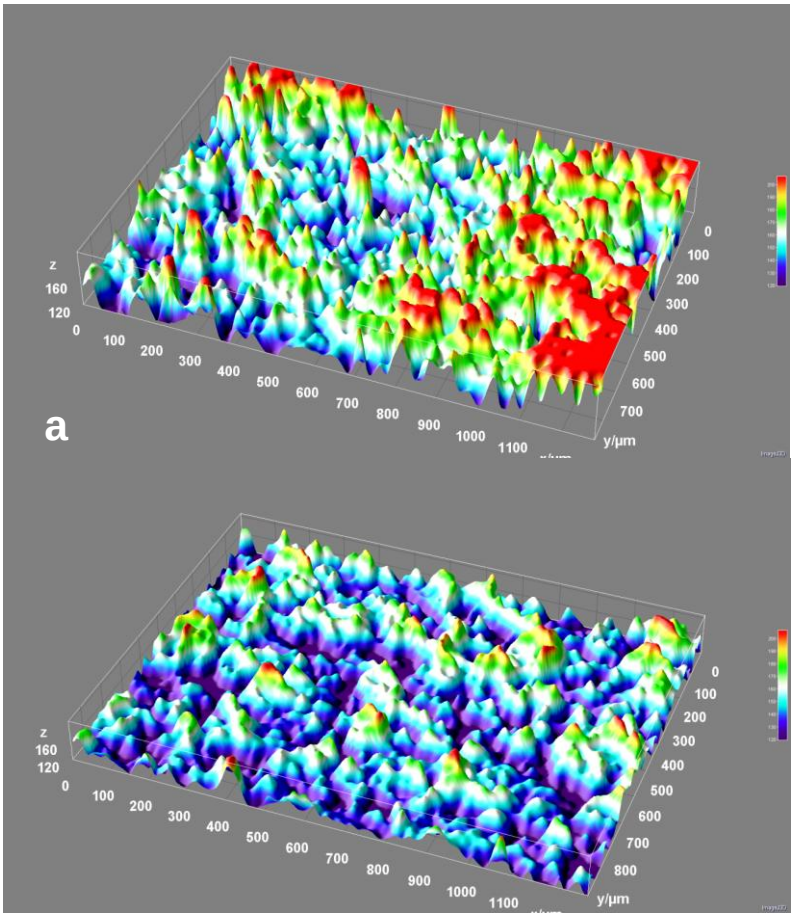

Figure 5. Typical 3D surface morphology of, a) as manufactured and, b) heat treated Ti6Al4V LAM component.

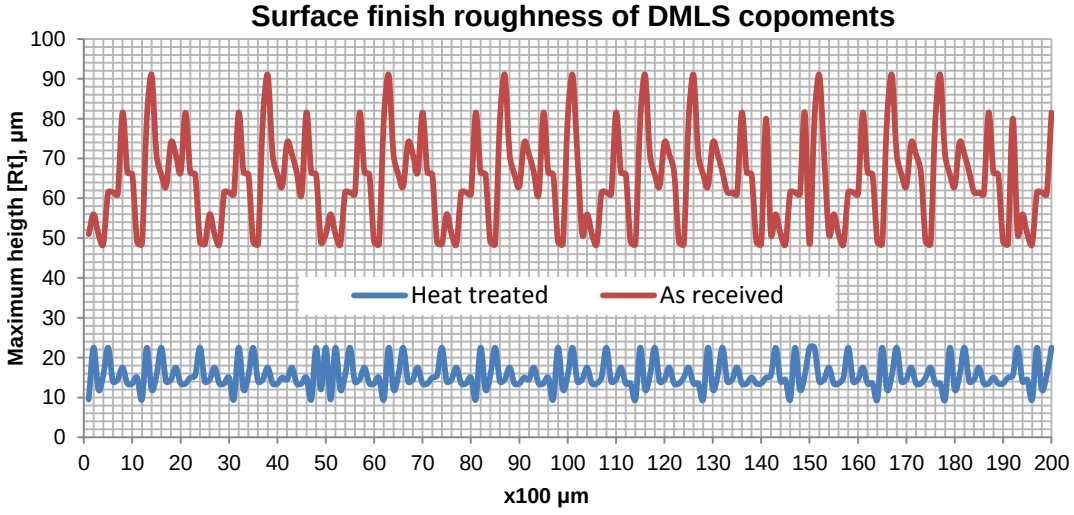

Figure 6. The maximum height (Rt) of the as manufactured (top graph) and heat treated Ti6Al4V LAM component

3.1.3. Microstructural analysis

The typical microstructure of the LAM Ti6Al4V component is shown in Figures 7 and 8. The microstructural analysis revealed columnar grains on XZ or YZ plan and equiaxed grains on XY plan. The powder/ laser beam interaction, scan velocity, and laser spot size determine the microstructure and size of the melt pool. Higher laser power and large spot size produces a mixture of columnar grains and equiaxed grains whereas fully columnar grains are produced when the reduced laser power and spot size are used [6, 7]. Low scanning velocity produces large melt pool, however high scanning velocity leads to the smaller melt pool [12]. When laser scanning is performed in different directions, the grain size distribution is bigger than when deposition is in the same direction for all layers [14]. Grain size tend to increase with increasing traverse speed and incident energy (IE) (IE=laser power/traverse speed) [6, 7]. Coarse grains are formed at the top layers due to slow cooling rate as building moves away from the base, see Figure 8a. Columnar are oriented at 90° to XY plan (Figure 7). Columnar grains with epitaxial growth on successive layers are due to high laser power and lower cooling rate.
Layer bands are also revealed in LAM component, see Figure 7 and 8a. It is caused by remelting of the already solidified Ti6Al4V during deposition of subsequent layers. For thin wall deposits, the cooling rate of the molten pool decreases with increasing deposit height [14]. The heat input distribution determines the geometry of the molten pool and the size the heat affected zone (HAZ) (Figure 8a). The temperature gradient is highest around the molten pool; hence the HAZ is concentrated near the laser focal zone. Low laser power results in a geometrically and dimensionally stable molten pool. Since heat transfer is mainly by conduction, heat extraction is rapid around the molten pool resulting in refined grains in the microstructure. Cooling will as well be rapid in the z-direction due to additional heat sink offered by the base [9].
Un-molten powder particles, shrinkage cavities (Figure 8c) and gas porosity (Figure 8b) observed in LAM part are due to rapid solidification rates (higher scanning speed), gas entrapment and remelting associated with the process [15].

Figure 7. Typical grain structure, of the LAM Ti6Al4V component, shown in 3D

The typical DSC thermogram of the as manufactured and heat treated Ti6Al4V sample is shown in Figure 9. During the first heating cycle of LAM sample, the orthorhombic martensite (α'') transformed into beta (β), α_2 into β, then after α into β at the transus temperature, and finally the hexagonal martensite (α') transformed into β. However the mil-annealed, as well as the second heating cycle revealed only the $\alpha_2 \rightarrow \beta$ and $\alpha \rightarrow \beta$ peaks. The reverse reaction for both cycles showed β into α transformation [18].

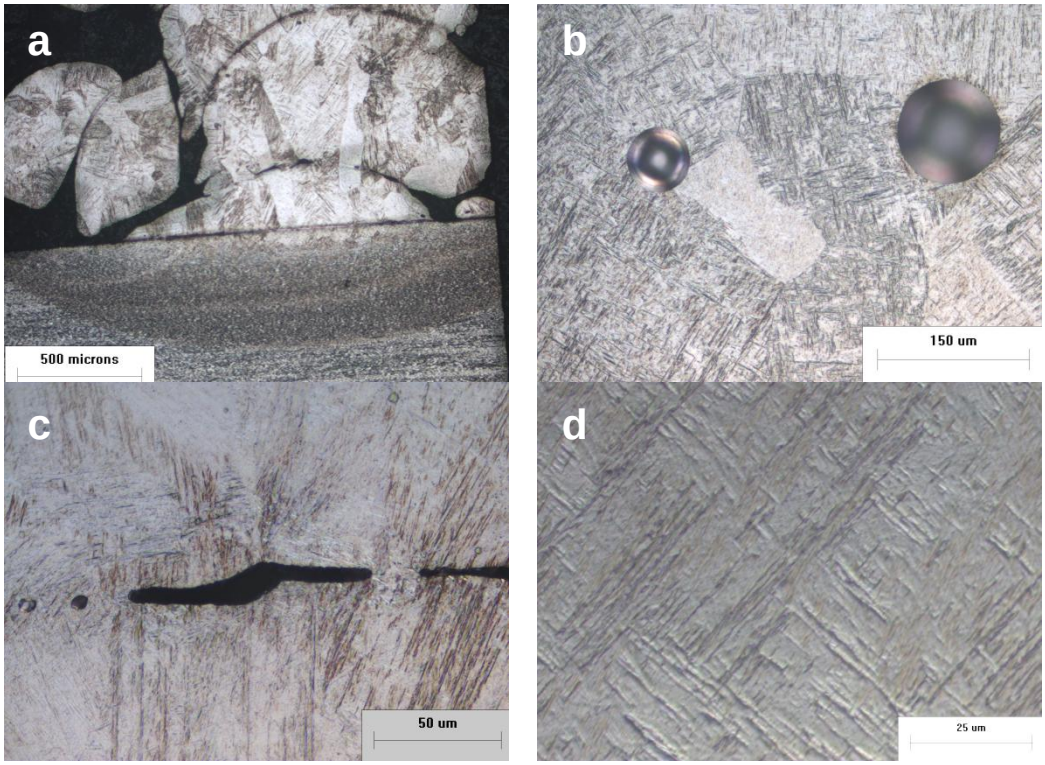

Figure 8. Typical defects revealed in Ti6Al4V LAM component, a) layer bands, b) gas pores, c) shrinkage cavities and, uncontrolled fully martensitic structure component

Martensitic structure is produced, due to small melt pools associated with higher cooling rate. This is the result of short laser–powder Ti6Al4V interaction time and localized heat input leading to steep thermal gradients in the component (resulting in thermal stress). Rapid cooling results in partial or full martensitic (α') structure whereas slow cooling results in lamellar structure. The cooling rate decreases as more layers are deposited due to built-in heat in the base and previous layers. The inert gas used in the building chamber determines the cooling rate due to differences in thermal conductivities. Helium has higher thermal conductivity (0.15 w/m.K) than Nitrogen (0.026 w/m.K), argon (0.018 w/m.k) and Krypton (0.00949 w/m.K) at elevated temperatures [16].

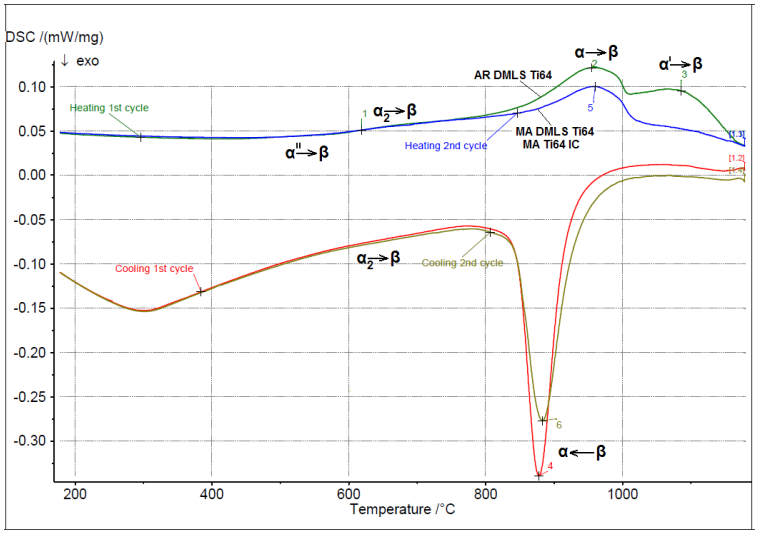

Figure 9. The typical DSC thermogram of the as received and heat treated Ti6Al4V sample

Higher laser power is initially (for first layers) required to compensate for heat sink by the cold base (See, Figure 8a), the power decreases as the component construction progresses.

At very high scanning velocity, the cooling rate is significantly higher initially but becomes uniform after deposition of the first few layers. High scanning speeds are however not preferable due to vulnerability to pore formation as a result of unmolten powder. Low scanning speeds result in continuously decreasing the cooling rate as construction progresses. Higher cooling rates result in fine grains and martensite structure and superior tensile properties of the LAM part [10].

3.2. Tensile properties and heat treatment response

The tensile properties (ultimate tensile stress (UTS), 0.2% offset yielding stress (Ys) and % Elongation) of the as received DMLS, as received-polished, mill annealed DMLS (MA 1 and MA 2 DMLS) and mill annealed investment cast (MA 1, MA 2 and MA 3 IC) of Ti6Al4V alloy, are shown in Figure 10. The as manufactured DMLS demonstrated relatively higher UTS, Ys and % elongation compared to the mil-annealed part (tensile stress applied in Z direction). Grinding or polishing the LAM component strongly improved the bulk tensile properties. This improvement is due to the removal of the external porous layer (Figure 11a). Tensile properties are dependent on operating conditions and characteristics of Ti6Al4V powder used. Pores (Figure 11b) act as crack nucleation sites thereby not only reducing the stress to produce plastic deformation; they suppress the nucleation and pile-up of dislocations.

Mil-annealing the LAM component effectively reduced the tensile properties. The bulk tensile properties increased as the mil-annealed temperature decreased. Contrary to the investment cast Ti6Al4V component [17], the mil-annealed treatment improved the Tensile. The UTS and Ys increased as the mil-annealing temperature increased, however the % elongation increased as the mil-annealing temperature decreased.
When the mil-annealing treatment of LAM component, is performed within the β-field, the hexagonal (α′) and orthorhombic martensite (α″) are transformed to mainly α/β lamellae structure. Below the β-Transus temperature, only the orthorhombic martensite transforms which may explain the increase of tensile properties in LAM component as the mil-annealing temperature increases. The heat treatment response of the LAM component is completely different compared to conventional manufactured parts [11].

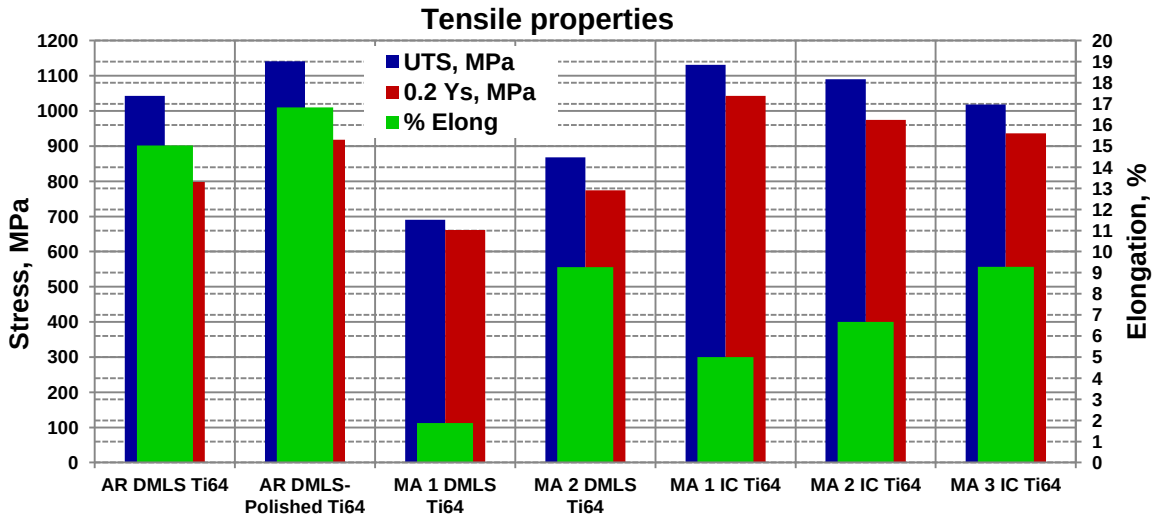

Figure 10. Tensile properties of the as manufactured, ground and heat treated DMLS component, and the investment cast component using the alloy Ti6Al4V

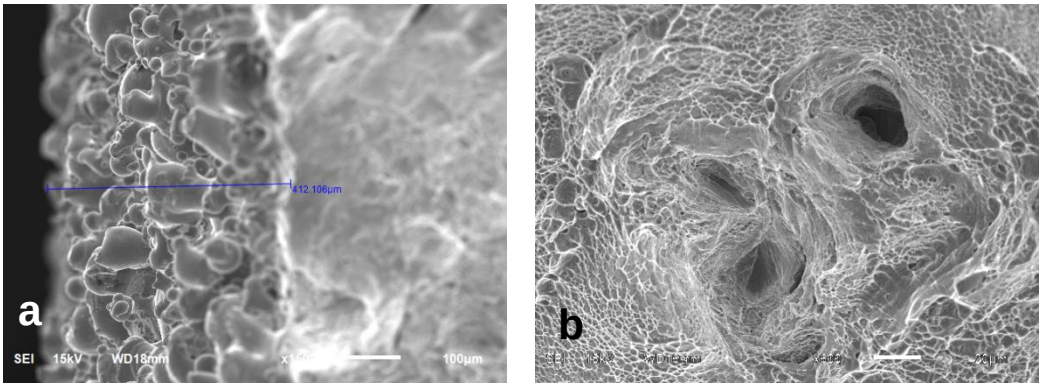

Figure 10. Tensile Fracture surface of the as manufactured Ti6Al4V DMLS component

4. Conclusions

The metallurgical evaluation of the LENS and DMLS Ti6Al4V components, in the as manufactured and mil-annealed conditions led to the following conclusions:

- The higher interfacial energy between the base and the first deposited layer was one of the causes of higher surface roughness and pores formation in the outer surface layer.
- The heat treatment in the vacuum furnace slightly improved the surface finish.
- A mixture of columnar grains, layer bands and fully martensite structure was developed during laser additive manufacturing process.
- Post-grinding or polishing of the laser manufactured component surely improved the tensile properties.
- A specific heat treatment process for laser manufactured Ti6Al4Vcomponent need to be design.

Acknowledgements

Authors acknowledge the technical and financial support of LM & NLC-CSIR (Light Metals & National Laser Centre-Council for Scientific and Industrial Research) and CUT (Central University of Technology).

References

1. B. Baufeld and Omer van der Biest, *Mechanical properties of Ti-6Al-4V specimen produced by shaped metal deposition*, Science and Technology of Advanced materials, 2009 (10), 1-10.
2. D.E. Cooper, M. Stanford, K.A.Kibble and G.J. Gibbons, "*Additive manufacturing for product improvement at Red Bull Technology*, "Materials and Design, 2012 (41), 226-230.
3. C. Sanz and V. Garcia Navas, "*Structural integrity of direct metal laser sintered parts subjected to thermal and finishing treatments*", Journal of Materials Processing Technology, 2013 (213) 2126-2136.
4. S. Leuders, M. Thone, A. Riemer, T. Niendorf, T. Troster, H.A. Richard and H.j. Maier, "*On the mechanical behaviour of titanium alloy Ti6Al4V manufactured by selective laser melting: Fatigure resistance and crack growth performance*", International Journal of Fatigue, 2013 (48), 300-307.
5. E. Brandl, A. Schoberth, C. Leyens, "*Morphology, microstructure and hardness of titanium (Ti-6Al-4V) blocks deposited by wire-feed additive layer manufacturing (ALM)*", materials Science and Engineering A, 2012, 295-307.
6. Kobryn P. A., Semiatin S. L., *The laser additive manufacture of Ti-6Al-4V,* JOM, 2001, 40-42.
7. Lewis G. K., Schlienger E., 2000, *Practical considerations and capabilities for laser assisted direct metal deposition*, Materials & Design 21 (200): 417-423

8. Griffith M. L., Keicher D. M., Atwood C. L., Harwell L. D., Greene D. L., Smugeresky J. E., Romeo J. A*., Free form fabrication of metallic components using laser engineered net shaping (LENS^{TM})*
9. Lavernia E. J., Riqing Y., Zhou Y., Zheng D., Smugeresky J. E., *Numerical modelling of the thermal behaviour during the LENS process, Materials Science and Engineering A, 428(2006):47-53*
10. Wang L., Felicelli S., Gooroochurn Y., Wang P. T., Horstemeyer M. F., *Optimization of the LENS process for steady molten pool size,*
11. Vrancken B., Thijs L., Kruth J. P., Van Humbeeck J., *Heat treatment of Ti6Al4V produced by Selective Laser Melting: Microstructure and mechanical properties, Journal of Alloy and Compounds 541 (2012): 177-185*
12. Murr L. E., Gaytan S. M., Ramirez A. D., Martinez E., Hernan dez J., Amato K. N., Shindo P. W., Medina F. R., Wicker R. B., **:** *Fabrication of Metal and Alloy Components by Additive Manufacturing: Examples of 3D Materials Science, Journal of Materials Research and Technology 01(2012): 42-54*
13. Boisselier D., Sankare S., *Influence of powder characteristics in laser direct metal deposition of SS316L for metallic parts manufacturing, Physics Procedia 39 (2012): 455-463*
14. Dinda G. P., Dasgupta A. K., Mazmder J., *Evolution of microstructure in laser deposited Al-11.28%Si alloy, Surface and Coatings Technology 206 (2012): 2152-2160*
15. Shishkovsky I., Missemer F., Smurov I., *Direct metal deposition of functional graded structures in Ti-Al system, Physics Procedia 39 (2012): 382-391.*
16. Murr L. E., Gaytan S. M., Ramirez A. D., Martinez E., Hernandez J., Amato K. N., Shindo P. W., Medina F. R., Wicker R. B., *Metal Fabrication by Additive Manufacturing using Laser and Electron Beam Melting Technologies, Journal of Materials Research and Technology 28.1(2012): 01-14*
17. Mutombo, K., Rossouw, P., Govender, G. *Mechanical Properties of Mill-Annealed Ti6Al4V Investment Cast*. Mat. Sc. Forum 2011(690) 69-72
18. Mutombo, K., Mazibuko, N.E., Siyasiya, C., Stumpf, W.E. *Phase evolution in T6Al4V alloy during thermal and themo-mechanical treatment.* RADASA 2012